JOURNAL OF SOLID STATE CHEMISTRY 113, 345–354 (1994)

Synthesis and Characterization of $K_{0.19}Ba_{3.81}Mo_{22}O_{34}$: A Quaternary Reduced Molybdenum Oxide Containing Metal–Metal Bonded Oligomers with Five Trans Edge-Shared Molybdenum Octahedra

George L. Schimek and Robert E. McCarley[1]

Ames Laboratory, USDOE, and Department of Chemistry, Iowa State University, Ames, Iowa 50011

Received November 17, 1993; accepted March 24, 1994

Crystals of $K_{0.19}Ba_{3.81}Mo_{22}O_{34}$, a metal–metal bonded oligomer in the series $M_{n-x}Mo_{4n+2}O_{6n+4}$ with $n = 5$, have been synthesized. The Mo_{22} clusters consist of five *trans* edge-shared Mo octahedra. The dominant features of $K_{0.19}Ba_{3.81}Mo_{22}O_{34}$ include four short and four long apical–apical Mo bond distances within the cluster, relatively long intercluster metal–metal bond distances (>2.99 Å), and cluster interconnections which have a stair–step arrangement from one Mo_{22} unit to the next. $K_{0.19}Ba_{3.81}Mo_{22}O_{34}$ crystallizes in the centrosymmetric space group $P2_1/a$, with lattice parameters of $a = 9.908(2)$ Å, $b = 9.353(2)$ Å, $c = 15.951(3)$ Å, $\beta = 98.78(2)°$, Vol = 1460.8(4) Å^3, $Z = 2$, and $R = 0.0493$ ($R_w = 0.0603$) for 2768 reflections with $I > 3.5\sigma(I)$. Five cations per formula unit can be accommodated in the pockets created by the interconnected $Mo_{22}O_{50}$ clusters. However, this phase has four fully occupied cation sites and one vacancy. The number of electrons available for metal–metal bonding (MCE) was derived from Mo–O bond valence sums around the molybdenum atoms (72(2)) and is in good agreement with the value calculated from formal oxidation states (71.8*e*). Mo–Mo bond order sums, excluding intercluster metal–metal interactions, although slightly high (MCE = 72.8(5)), indicate maximum utilization of electrons for Mo–Mo bonding. The magnetic susceptibility of this compound indicates that it is spin-paired with a small paramagnetic tail at low temperatures and a large residual χ_{TIP} above 50 K. Electron spin resonance results indicate that the paramagnetic tail may be arising from molybdenum containing impurities, or defects, on which electrons are trapped. Structural and electronic comparisons to two known pentameric oligomers are discussed. © 1994 Academic Press, Inc.

INTRODUCTION

The synthesis of compounds containing Mo chain-segment oligomers, $M_{n-x}Mo_{4n+2}O_{6n+4}$, appears to become increasingly more difficult as n, the number of *trans* edge-shared molybdenum octahedra, becomes larger. The thermodynamic stability of large oligomeric members, with respect to smaller members, or the $n = \infty$ (infinite chain) $M_xMo_4O_6$ (1–9) members, must then necessarily be small. Thus, the preparation of such materials becomes increasingly sensitive to such factors as cation choice, optimal cluster electron count, starting reagents, and reaction temperatures. To date, only one synthetic route and a relatively poor single crystal X-ray structure refinement ($R = 0.095$) have been reported for an oligomer with five *trans* edge-shared Mo octahedra, $In_6Mo_{22}O_{34}$ (10). Six cations are accommodated in this $n = 5$ oligomer since indium prefers a square planar coordination environment by its surrounding oxygen atoms. The structural model for this indium pentameric oligomer, reported by Simon and co-workers, describes the basic framework correctly. However, bond distances and angles of the structure have rather large standard deviations. This poor refinment is thought to be due to the presence of domains, or intergrowth, of oligomers with varying modes of cluster length and/or interconnection. An earlier study of the In–Mo–O system by Simon's group showed that $In_{11}Mo_{40}O_{62}$ (11) could also be prepared. This remarkable compound contains a one to one ratio of $n = 4$ and 5 oligomers. Efforts in this laboratory have yielded another pentameric oligomer with a much-improved structural refinement. The synthesis and characterization of $K_{0.19}Ba_{3.81}Mo_{22}O_{34}$ are discussed. This $n = 5$ oligomer was studied by single crystal X-ray structure refinements, microprobe analyses, magnetic susceptibility, and electron spin resonance (ESR).

EXPERIMENTAL

Synthesis. The starting reagents included K_2MoO_4, $BaMoO_4$, MoO_3, and Mo. Potassium molybdate was prepared by reacting KOH (Fisher Certified A.C.S.) with a stoichiometric quantity of MoO_3 in deionized water. The molybdate solution was filtered, the volume reduced by heating, and the product collected on a glass frit. The wet molybdate was dried at 120°C overnight under dynamic vacuum. Barium molybdate was prepared by mixing an

[1] To whom correspondence should be addressed.

0022-4596/94 $6.00
Copyright © 1994 by Academic Press, Inc.
All rights of reproduction in any form reserved.

aqueous solution of barium chloride dihydrate (Baker Analyzed Reagent, 99.6%) with an aqueous solution containing a stoichiometric quantity of sodium molybdate dihydrate (Fisher Certified). The white precipitate was filtered, washed with copious amounts of distilled water, and then dried overnight at 130°C under dynamic vacuum. Molybdenum trioxide was dried at 520°C overnight in an open crucible and then cooled over desiccant. Molybdenum powder (Aldrich, 99.99%) was dried under dynamic vacuum at 120°C overnight. All the starting reagents subsequently were stored in a desiccator. Molybdenum tubing (Thermoelectron Corp., 99.97%) was cleaned by heating at 950°C for 5 hr under flowing hydrogen gas. After cooling to room temperature in a hydrogen atmosphere, the tubing was also stored over desiccant.

Attempts to prepare the quaternary $K_2Ba_2Mo_{18}O_{28}$ resulted instead in the formation of the title oligomeric member, the pentameric $K_{0.19}Ba_{3.81}Mo_{22}O_{34}$. The correct stoichiometric mole ratios of K_2MoO_4, $BaMoO_4$, MoO_3, and Mo necessary to prepare the tetrameric oligomer had been thoroughly ground, pressed into a pellet, and loaded into a molybdenum tube. The tube and contents were evacuated ($\sim 1 \times 10^{-4}$ Torr), fired at 150°C for 20 min, and left under dynamic vacuum overnight before being sealed under vacuum ($\sim 2 \times 10^{-5}$ Torr) by electron beam welding. The sample was fired overnight at 1400°C in a high-temperature vacuum furnace and then further reacted at 1500°C for another 119 hr. The furnace was cooled at an average rate of 1°C/min down to 1240°C, 2°C/min to 1000°C, 5°C/min to 800°C, and then furnace-cooled to 100°C in approximately 1 hr. Upon opening, the interior Mo tube walls were found to be clean. The pellet was a coarse mixture of black, chunk-like crystals ($n = 5$ oligomer), black powder (MoO_2), and silver beads (Mo).

Unfortunately, single-phase preparation of $K_{0.19}Ba_{3.81}Mo_{22}O_{34}$ has not been achieved. As observed in previous synthetic routes to oligomeric members, $M_{n-x}Mo_{4n+2}O_{6n+4}$ (12), in which potassium was utilized, preparation of these phases appears to be promoted in the presence of excess K_2MoO_4. The potassium molybdate, or its decomposition products, appear to act as good fluxes. Thus, over the course of the reaction, potassium may be incorporated into the structure with a wide range of concentrations. In this case, the pentameric oligomer only incorporates a small amount of potassium. At 1500°C, the constituent $BaMoO_4$ (mp = 1480°C) could also act as a flux. Thus the product obtained is not necessarily a line compound or even composed of only $n = 5$ oligomers. By refinement on the occupancy of K and Ba positions, the overall composition, $K_{0.19}Ba_{3.81}Mo_{22}O_{34}$, was determined by the single crystal structure determination. Subsequent quantitative determination of K, Ba, and Mo by electron microprobe X-ray emission analyses of four small crystals with a total of five data points resulted in the net composition $K_{0.09(2)}Ba_{3.6(2)}Mo_{22}O_{33.9(1)}$ in reasonable agreement with that from the structure determination. This stoichiometry is derived from a fixed number of molybdenums and the oxygen content was then calculated by difference.

TABLE 1
X-ray Powder Diffraction Data for $K_{0.19}Ba_{3.81}Mo_{22}O_{34}$

d-Spacing (Å)			
Observed	Calculated[b]	Intensity[a]	*hkl*
6.790	6.763	100	110
4.884	4.896, 4.892	20	200, $\bar{2}01$
4.884	4.885	20	$11\bar{2}$
4.700	4.677	20	020
4.235	4.220	10	120
3.574	3.573	18	$\bar{1}14$
3.387	3.382, 3.380	13	220, $\bar{2}21$
3.120	3.110	50	$\bar{3}11$
3.080	3.082	22	310
2.982	2.970	74	$\bar{1}30$
2.705	2.695	23	$\bar{3}21$
2.517	2.516, 2.505	11	$\bar{3}23$, 313
2.478	2.478, 2.477	25	$\bar{2}06$, $\bar{4}01$
2.463	2.450	64	125
2.405	2.401	51	$\bar{2}15$
2.397	2.395	77	$\bar{2}16$
2.281	2.299	68	$\bar{1}26$
2.198	2.194	19	225
2.192	2.189	15	$\bar{2}26$
2.172	2.188	34	$\bar{4}21$
2.047	2.060	26	$\bar{3}15$
2.017	2.005	35	$\bar{3}26$
1.948	1.943, 1.940	36	235, $\bar{2}36$
1.942	1.939, 1.938	77	$\bar{4}31$, $\bar{5}11$
1.915	1.925	50	$\bar{3}25$
1.712	1.703, 1.701	28	245, $\bar{2}46$
1.703	1.700	59	$\bar{4}41$

[a] Relative intensity.
[b] *d*-Spacings were calculated from the refined monoclinic cell parameters determined from single crystal indexing: $a = 9.908(2)$ Å, $b = 9.353(2)$ Å, $c = 15.951(3)$ Å, and $\beta = 98.78(2)°$.

X-ray Guinier powder diffraction. An Enraf Nonius Delft FR552 triple-focusing Guinier X-ray powder diffraction camera was used with Cu$K\alpha_1$ radiation ($\lambda = 1.540562$ Å) generated from an AEG fine-focus tube powered by a General Electric XRD-5 generator. National Bureau of Standards silicon powder was used as an external standard. Table 1 lists 27 *d*-spacings which could be indexed as belonging to the pentameric oligomer. These results were obtained from well-ground, hand-selected crystals.

X-ray single crystal data collection. A black crystal of $K_{0.19}Ba_{3.81}Mo_{22}O_{34}$ with ill-defined geometry and dimensions of $0.07 \times 0.12 \times 0.12$ mm^3 was mounted with epoxy cement on a glass fiber for data collection. A Rigaku

AFC6R rotating anode diffractometer was used with graphite monochromated Mo$K\alpha$ radiation (λ = 0.71069 Å) generated at 7 kW. Monoclinic lattice parameters and an orientation matrix for data collection were derived from 13 randomly located and centered reflections with a two theta range of 13–16°. Rotation photographs about the three crystallographic axes indicated the absence of twinning and reflections arising from any superstructural effects. A refinement on 25 reflections with strong intensity and two theta values near 40° gave a final idealized cell with the following lattice parameters: a = 9.908(2) Å, b = 9.353(2) Å, c = 15.951(3) Å, β = 98.78(2)°, and volume = 1460.8(4) Å^3. Three standard reflections were measured every 150 reflections and showed no apparent variation in intensity during the data collection. Data were collected, at room temperature from 0 to 60° in two theta in the hemisphere ($\pm h$, k, $\pm l$), using an ω-2θ scan mode. The number of reflections measured was 9042, of which 6212 were unique ($I > 3\sigma(I)$), R_{int} = 4.0%, and 2768 were observed with $I > 3.5\sigma(I)$. The linear absorption coefficient for Mo$K\alpha$ was 136.91 cm^{-1}. An empirical absorption correction (13) was applied based upon five azimuthal scans of reflections with an average transmission range of 0.942–1.000. The intensity data were corrected for Lorentz and polarization effects.

Structure solution and refinement. The space group $P2_1/a$ (#14) was chosen based on the systematic absences of $h0l$: $h \neq 2n$ and $0k0$: $k \neq 2n$, however, there was one violation of the latter condition which could be attributed to a very intense neighboring reflection and 49 violations of the former condition, none of which could be validly excluded. Therefore, the structure was solved in three space groups by direct methods using SHELXS[14]: $P2_1/a$ (0.055), $P2_1$ (0.041), and Pa (0.034). The structure was refined in $P2_1/a$ and Pa on $|F|$ by full matrix, least squares techniques (15) with the TEXSAN (16) package.

The refinement in Pa (#7, $h0l \neq 2n$) converged at R = 7.3%. In this space group, all the atoms in the formula unit are unique, thereby allowing distortions to occur that do not necessitate an inversion related contribution to another part of the same cluster. The distortions that occurred within the cluster were only slightly different than the more symmetrical solution in $P2_1/a$. Thus the centrosymmetric space group $P2_1/a$ was chosen to be a more valid model, with the realization that small distortions presumably do occur, but do not contribute significantly to the intensity of the measured data.

Using $P2_1/a$ (#14) as the space group, about half of the molybdenum atoms were located in the initial output from direct methods. After refining on these positions, the remaining molybdenum atom positions were found in a Fourier electron difference map. The molybdenum atom positions refined to R = 41%. Two very large peaks remained in the difference map and these were assigned as barium cations. Inclusion of these two atoms resulted in a refinement at 18%. The two cations were allowed to refine as a combination of potassium and barium, since microprobe analyses indicated that both cations were present in other crystals from the same reaction product. These conditions converged at R = 12%. After locating and positionally refining the unique oxygen atoms, all the thermal parameters of the heavy atoms were then allowed to refine isotropically; this resulted in R = 8.1%. After refining the oxygen atom thermal parameters isotropically, the R factor was 7.0%. Anisotropic refinement of the thermal parameters for the heavy atoms and eight of the oxygen atoms converged at R = 6.2%. A secondary extinction correction was applied (5.6(9) × 10^{-8}) and cation occupancies were rechecked. The final cycle converged at R = 0.0493 and R_w = 0.0603. The final occupancies indicated that the two cation sites were fully occupied, with Ba1/K1 at 95.1/4.9(7)% and Ba2/K2 at 95.6/4.4(7)%, in good agreement with the quantitative microprobe analyses. However, the site at the origin, the central available cation position, was determined to be completely vacant. The thermal parameters of the potassium atoms were fixed to the anisotropic values derived for the respective barium cations. All the thermal parameters for the molybdenum, barium, and 8 of the 17 oxygen atoms were refined anisotropically. A final electron difference map was not devoid of electron density, since there were 10 peaks with electron density between 10.1 and 7.4 e/Å^3. All peaks were located within the cation pockets and had cation to peak distances ranging from 1.7 to 2.2 Å. No strongly convincing arguments can be made to explain the considerable quantity of electron density remaining. The application of an absorption correction derived from a series of Ψ-scans indicated T_{min} = 0.942. An empirical DIFABS (17) correction on isotropically refined data, or a cylindrical absorption correction based upon crystal size, indicated no significant improvement as compared to the current refinement model. Therefore absorption most likely was not the cause of the residual electron density. Another possibility is that the current assessment of the cation locations in the pockets is not complete. It is peculiar that the central cation site, which should be ideal for potassium, is left vacant. A third scenario, and perhaps the most realistic possibility, is that the crystal is intergrown with regions where there are oligomers with different chain lengths and/or modes of interconnection. This behavior was observed in the In–Mo–O system studied by Simon (18). Given the quality of the refinement, the crystal used for data collection is probably composed of essentially, although not completely, Mo_{22} units interconnected in a stair-step fashion.

Details of the data collection and refinement for $K_{0.19}Ba_{3.81}Mo_{22}O_{34}$ are given in Table 2. Final positional

TABLE 2
X-ray Crystallographic Data for $K_{0.19}Ba_{3.81}Mo_{22}O_{34}$

Formula	$K_{0.19}Ba_{3.81}Mo_{22}O_{34}$
Formula weight	3185.32
Crystal system	monoclinic
Space group	$P2_1/a$ (#14)
a (Å)	9.908(2)
b (Å)	9.353(2)
c (Å)	15.951(3)
β (degrees)	98.78(2)
Volume (Å^3)	1460.8(4)
Z	2
Calculated density (g/cm^3)	7.172
Crystal size (mm^3)	0.07 × 0.12 × 0.12
μ(Mo$K\alpha$) (cm^{-1})	136.91
Diffractometer	Rigaku AFC6R
λ, Å, graphite monochromator	0.71069
Temperature (°C)	24
2θ range (degrees)	0–60
Scan mode	ω-2θ
No. reflections collected	9042
No. observations ($I > 3.5\sigma(I)$), (unique, $I > 3\sigma(I)$)	2768 (6212)
No. variables	229
Quality of fit[a]	2.138
Max. shift in final cycle	0.002
Largest peaks in final diff. map (e/Å^3)	+10.1, −3.9
Transmission coefficient	0.942–1.000
R[b], R_ω[c]	0.0492, 0.0603

[a] Quality of fit = $[\Sigma\omega\{|F_0| - |F_c|\}^2/\{N_{obs} - N_{parameters}\}]^{1/2}$
[b] $R = \Sigma||F_0| - |F_c||/\Sigma|F_0|$.
[c] $R_\omega = [\Sigma\omega\{|F_0| - |F_c|\}^2/\Sigma\omega|F_0|^2]^{1/2}$; $\omega = 1/\sigma^2\{|F_0|\}$.

TABLE 3
Atomic Coordinates for $K_{0.19}Ba_{3.81}Mo_{22}O_{34}$

Atom[a]	X	Y	Z	B_{eq}[b]
Ba1/K1[c]	0.91910(8)	0.0072(1)	0.11851(5)	0.58(3)
Ba2/K2[c]	0.96132(8)	0.0005(1)	0.34553(6)	0.63(3)
Mo1	0.6072(1)	0.1280(1)	0.30985(7)	0.24(4)
Mo2	0.5635(1)	0.8879(1)	0.41055(7)	0.24(4)
Mo3	0.5221(1)	0.8798(1)	0.23092(7)	0.23(4)
Mo4	0.3001(1)	0.8690(1)	0.31198(8)	0.43(4)
Mo5	0.3438(1)	0.1165(1)	0.23082(7)	0.21(4)
Mo6	0.5663(1)	0.1233(1)	0.14431(7)	0.21(4)
Mo7	0.3928(1)	0.1128(1)	0.41011(7)	0.19(4)
Mo8	0.4673(1)	0.8797(1)	0.05567(8)	0.52(4)
Mo9	0.6543(1)	0.1290(1)	0.50139(8)	0.28(4)
Mo10	0.2570(1)	0.8679(1)	0.14266(8)	0.33(4)
Mo11	0.3014(1)	0.1148(1)	0.05765(7)	0.22(4)
O1	0.675(1)	0.765(1)	0.5012(6)	0.4(1)
O2	0.465(1)	0.238(1)	0.0420(6)	0.5(3)
O3	0.1730(9)	0.994(1)	0.2288(6)	0.4(1)
O4	0.639(1)	0.005(1)	0.0451(6)	0.4(1)
O5	0.310(1)	0.743(1)	0.0468(6)	0.6(1)
O6	0.497(1)	0.269(1)	0.2246(6)	0.4(3)
O7	0.368(1)	0.730(1)	0.2290(7)	0.8(3)
O8	0.631(1)	0.757(1)	0.3218(6)	0.5(1)
O9	0.7290(9)	0.018(1)	0.4102(6)	0.3(3)
O10	0.6955(9)	0.004(1)	0.2288(6)	0.3(1)
O11	0.555(1)	0.251(1)	0.4080(6)	0.5(1)
O12	0.237(1)	0.247(1)	0.1352(6)	0.6(3)
O13	0.403(1)	0.746(1)	0.4108(6)	0.7(3)
O14	0.781(1)	0.258(1)	0.3163(6)	0.4(1)
O15	0.582(1)	0.754(1)	0.1382(6)	0.5(3)
O16	0.226(1)	0.984(1)	0.4083(7)	0.9(4)
O17	0.147(1)	0.991(1)	0.0488(6)	0.6(1)

[a] All atoms reside on the Wyckoff position 4e.
[b] The equivalent isotropic temperature factor, B_{eq}, is defined as $8\pi^2/3\{\Sigma_i\Sigma_j(U_{ij}a_i^*a_j^*\vec{a}_i\vec{a}_j)\}$, where the summations of i and j range from 1 to 3.
[c] Ba1 and K1 reside on the same site with 95.1(7) and 4.9(7)% occupancies, respectively. Ba2 and K2 reside on the same site with 95.6(7) and 4.4(7)% occupancies, respectively.

parameters and isotropic temperature factors are listed in Table 3.

Magnetic susceptibility. The magnetic properties were examined on two samples of selected crystals taken from separate reactions. A Quantum Design SQUID magnetosusceptometer was utilized. The samples were loaded into 3 mm inner diameter fused silica tubes that had been sealed on the bottom half with 3 mm outer diameter fused silica rods. Another fused silica rod was placed on top of each of the samples, thus giving an arrangement where a uniform measurement could be made. The data were subsequently corrected for the diamagnetic contribution of the quartz.

Electron spin resonance. X-band ESR spectra were recorded on well-ground crystals of $K_{0.19}Ba_{3.81}Mo_{22}O_{34}$ with a Bruker ER200-SRC instrument equipped with an Oxford Instruments ESR 900 flow-through cryostat and a DTC-2 digital temperature controller. A Hewlett-Packard 5342 microwave frequency recorder was used to measure the exact frequency of the microwave radiation. The data to be described were averaged over five scans and collected using a modulation frequency of 100 kHz and a modulation amplitude of 3.2 Gauss. The instrument was calibrated against weak pitchblende prior to use.

RESULTS AND DISCUSSION

Description of structure. $K_{0.19}Ba_{3.81}Mo_{22}O_{34}$ can be described as a framework of molybdenum oxide cluster units in which five *trans* edge-shared molybdenum octahedra have all edges bridged by oxygen and all apical Mo atoms capped by oxygen. An ORTEP drawing of this building block, the $Mo_{22}O_{50}$ unit, is shown in Fig. 1 (19). A prominent feature of this unit, within the strong metal–metal bonded framework, is the pairwise distortion of the apical molybdenum atoms which give rise to a short-long-long-short arrangement of Mo–Mo bond distances: 2.610(2) Å for Mo1–Mo6, 3.019(2) Å for Mo1–Mo9, 2.942(2) Å for Mo4–Mo9, and 2.669(2) Å for Mo4–Mo10.

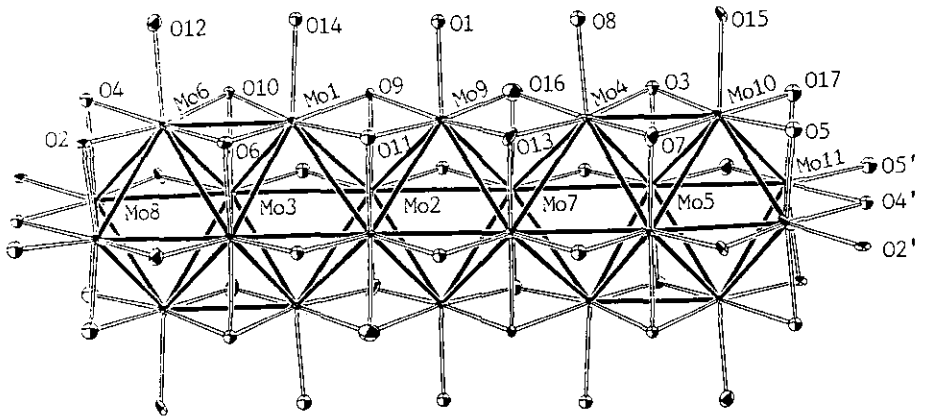

FIG. 1. An ORTEP drawing (70% thermal ellipsoids) of the $n = 5$ metal oxide cluster unit in $K_{0.19}Ba_{3.81}Mo_{22}O_{34}$, as it is found parallel to the c axis.

The short apical–apical bond distances constitute the strongest metal–metal bonds within the cluster. These apical bond distances are similar to those reported by Simon (11) for the apical–apical interactions within the $[Mo_{22}O_{34}]^{8-}$ cluster found in $In_{11}Mo_{40}O_{62}$: 2.749, 2.938, 2.938, and 2.749 Å. However, the values for the K–Ba member are in sharp contrast to the reported apical–apical distances across the top of the $[Mo_{22}O_{34}]^{8-}$ cluster of $In_6Mo_{22}O_{34}$ (10): 2.834(10), 2.893(13), 2.893(13), and 2.834 (10) Å. Yet, the distances across the bottom of $In_6Mo_{22}O_{34}$ are similar to the K–Ba member: 2.673(10), 2.992(12), 2.992(12), and 2.673(10) Å. The angles between adjacent basal plane molybdenum atoms running parallel to the c axis (the chain direction) in $K_{0.19}Ba_{3.81}Mo_{22}O_{34}$ indicate only a small component of tilting: Mo8–Mo3–Mo2 at 176.68(5)°, Mo3–Mo2–Mo7 at 178.27(6)°, Mo2–Mo7–Mo5 at 178.79(5)°, and Mo7–Mo5–Mo11 at 178.52(5)°. Therefore, the apical–apical interactions observed are basically pairwise distortions of the apical molybdenum atoms formed by displacement of these atoms along the c direction.

Extended Hückel calculations by Hoffmann and Wheeler (20) on the clusters that make up $In_{11}Mo_{40}O_{62}$ indicate that such a pairwise distortion on the apical molybdenum bond distances in the Mo_{22} unit does not change the HOMO-LUMO gap. However, two molecular orbitals that contribute significantly to apical–apical bonding are lowered in energy by approximately 0.1 eV with this type of distortion.

The variation of the bond distances between the *trans* edge-shared molybdenum atoms follows the trend observed in $Ba_3Mo_{18}O_{28}$ (21) and $In_{11}Mo_{40}O_{62}$ (11). This trend indicates that the shared edge between the upper and lower apical–apical Mo bonds will be shorter than the average shared-edge Mo–Mo bond distance if the apical–apical distances are long, and vice versa. For $K_{0.19}Ba_{3.81}Mo_{22}O_{34}$, the shared-edge Mo–Mo bond distances (and apical–apical bond distances) are 2.832(2) Å for Mo3–Mo5′ (2.610(2) Å and 2.669(2) Å), and 2.698(2) Å for Mo2–Mo7′ (3.019(2) Å and 2.942(2) Å). The bond distances of the basal edges of the molybdenum octahedra that run parallel to the chain in $K_{0.19}Ba_{3.81}Mo_{22}O_{34}$ also follow the general trend observed in the oligomeric series, $M_{n-x}Mo_{4n+2}O_{6n+4}$ (10–12, 21, 22), that is, shorter metal–metal bond distances at the ends of the cluster (2.730(2) Å for Mo5–Mo11 and 2.765(2) Å for Mo3–Mo8) and longer bond distances toward the center of the cluster (2.827(2) Å for Mo5–Mo7 and Mo2–Mo7, and 2.833(2) Å for Mo2–Mo3). A complete listing of all the metal–metal bond distances can be found in Table 4.

The clusters in $K_{0.19}Ba_{3.81}Mo_{22}O_{34}$ are interconnected along the chain direction in the same stair-step fashion observed for all the oligomeric members with two, three, or four edge-sharing octahedra. This mode of interconnection is shown in Fig. 2. The stair-step arrangement of clusters is not observed for $In_{11}Mo_{40}O_{62}$ or $In_6Mo_{22}O_{34}$, which are interconnected in a zigzag fashion. The principal difference between these two modes is that the stair-step oligomers crystallize with a monoclinic lattice and the zigzag oligomers have an orthorhombic lattice. The intercluster bond distances for $K_{0.19}Ba_{3.81}Mo_{22}O_{34}$ are indicative of clusters that have only a small metal–metal interaction, 2.998(3) Å for Mo8–Mo8′, 3.128(2) Å for Mo8–Mo11′, and 3.156(2) Å for Mo6–Mo8′. Thus the clusters tend to be isolated units connected via Mo–O bonds.

The average intracluster Mo–Mo bond distance is 2.776 Å, quite comparable to the 2.798 Å found in both of Simon's Mo_{22} clusters (10, 11). This result appears to be consistent with the apparent charges on the cluster frameworks, and therefore, also results in a similar number of electrons available for metal–metal bonding. The $Mo_{22}O_{34}$

TABLE 4
Metal–Metal Interatomic Distances (Å) for $K_{0.19}Ba_{3.81}Mo_{22}O_{34}$[a]

Mo1–Mo2	2.832(2)	Mo1–Mo3	2.713(2)
Mo1–Mo5′	2.722(2)	Mo1–Mo6	2.610(2) apical[b]
Mo1–Mo7′	2.851(2)	Mo1–Mo9	3.019(2) apical
Mo2–Mo3	2.833(2)	Mo2–Mo4′	2.839(2)
Mo2–Mo7′	2.698(2)	Mo2–Mo7	2.827(2)
Mo2–Mo9	2.753(2)	Mo2–Mo9′	2.756(2)
Mo3–Mo4′	2.718(2)	Mo3–Mo5′	2.832(2)
Mo3–Mo6	2.734(2)	Mo3–Mo8	2.765(2)
Mo3–Mo10′	2.786(2)	Mo4–Mo5	2.720(2)
Mo4–Mo7	2.838(2)	Mo4–Mo9	2.942(2) apical
Mo4–Mo10	2.669(2) apical	Mo5–Mo6′	2.774(2)
Mo5–Mo7	2.827(2)	Mo5–Mo10	2.785(2)
Mo5–Mo11	2.730(2)	Mo6–Mo8	2.780(2)
Mo6–Mo8′	3.156(2) inter[c]	Mo6–Mo11′	2.774(2)
Mo7–Mo9′	2.743(2)	Mo7–Mo9	2.775(2)
Mo8–Mo8′	2.998(3) inter	Mo8–Mo10′	2.676(2)
Mo8–Mo11′	2.748(2)	Mo8–Mo11′	3.128(2) inter
Mo10–Mo11	2.747(2)	Ba1 · Ba1′[d]	4.328(1) inter
Ba1 · Ba2[d]	3.582(1)	Ba2 · Ba2′[d]	4.870(2)

[a] Atoms with primed numbers are related to those with unprimed numbers by the inversion center.
[b] Apical–apical Mo–Mo bond distances.
[c] Intercluster Mo–Mo bond distances.
[d] Occupancy of these cation positions combines both potassium and barium.

framework is formally 7.81- in the K–Ba member and reported as 8- in both of Simon's clusters.

The Mo–O bond distances have the typical range, with the shortest at 1.91(1) Å for Mo11–O17 and the longest at 2.21(1) Å for Mo11–O5′. As has been observed in reported oligomers (12, 21), these two extreme distances occur in the region where intercluster bonding occurs. All the Mo–O bond distances are given in Table 5.

The coordination environments for the cations are shown in Fig. 3. Note that O1, in the waist-bridging and apical-capping positions of the central molybdenum octahedron, does not participate in any other bonding, since the central cation site is vacant. The outer cation site, Ba1/K1, is coordinated by 11 oxygens ranging from 2.65(1) Å for Ba1/K1–O17 to 3.032(9) Å for Ba1/K1–O10, although five of these cation–oxygen bonds are significantly shorter than the others. The arrangement of these five oxygen atoms is irregular and does not constitute a simple geometric coordination sphere. Ba2/K2, the inner cation site, is ten-coordinate in oxygen, ranging from 2.63(1) Å for Ba2/K2–O13 to 3.010(9) Å for Ba2/K2–O3. Again, however, four of these bonds are less than 2.7 Å, thereby giving a coordination environment in which the cation resides at the top of a square pyramid. The four short Ba2/K2–O bonds are all oriented toward the center of the cation pocket, the location where the central cation vacancy is found. Thus, the observed arrangement is expected as the cations repeal each other and Ba2/K2 relaxes toward the vacancy. A complete listing of the cation–oxygen bond distances can also be found in Table 5. The rather large cation–cation distances, as listed in Table 4, reflect the minimized repulsions and are indicative of isolated ions (23).

$K_{0.19}Ba_{3.81}Mo_{22}O_{34}$ can be described by the following connectivity formula, $[M_{5-x}]^{y+}[(Mo_{22}O^{i}_{18}O^{i-i}_{4/2}O^{i-a}_{14/2})O^{a-i}_{14/2}]^{y-}$. Oxygen atoms O3, O6, O7, O9, O10, O11, O13, O16, and O17 are edge-bridging only within the cluster unit and are labeled O^{i}. The oxygen atoms corresponding to O^{i-i} are edge-sharing between neighboring clusters;

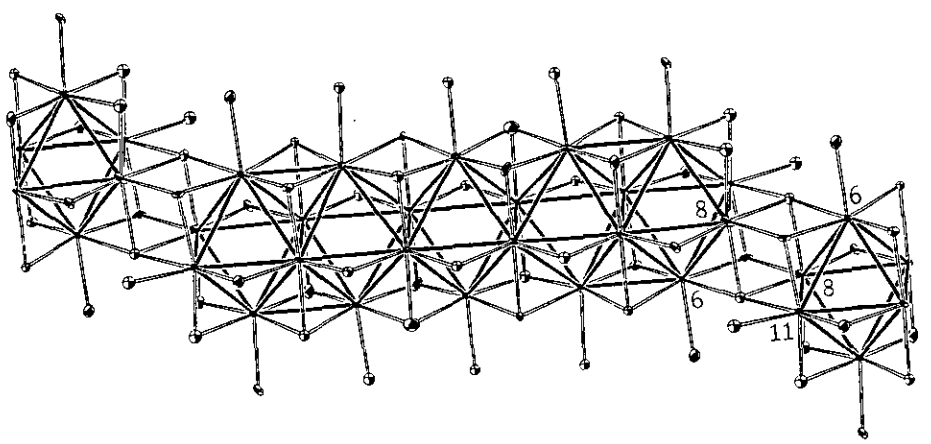

FIG. 2. An ORTEP drawing (70% thermal ellipsoids) emphasizing the stair-step interconnection of the metal oxide cluster units in $K_{0.19}Ba_{3.81}Mo_{22}O_{34}$. The chains propagate parallel to the c axis.

TABLE 5
Metal–Oxygen Bond Distances (Å) for $K_{0.19}Ba_{3.81}Mo_{22}O_{34}$[a]

Mo1–O6	2.081(9)	Mo1–O9	2.117(9)
Mo1–O10	2.031(9)	Mo1–O11	2.07(1)
Mo1–O14	2.097(9)	Mo2–O1′	2.03(1)
Mo2–O8′	2.06(1)	Mo2–O9	2.045(9)
Mo2–O13′	2.07(1)	Mo3–O7′	2.07(1)
Mo3–O8′	2.03(1)	Mo3–O10	2.078(9)
Mo3–O15′	2.049(9)	Mo4–O3	2.048(9)
Mo4–O7	2.04(1)	Mo4–O8	2.07(1)
Mo4–O13	2.09(1)	Mo4–O16	2.10(1)
Mo5–O3	2.042(9)	Mo5–O6′	2.091(9)
Mo5–O12′	2.10(1)	Mo5–O14′	1.97(1)
Mo6–O2	2.08(1)	Mo6–O4	2.15(1)
Mo6–O6	2.06(1)	Mo6–O10	2.044(9)
Mo6–O12	2.11(1)	Mo7–O1′	2.01(1)
Mo7–O11′	2.07(1)	Mo7–O14′	2.10(1)
Mo7–O16	2.05(1)	Mo8–O2′	2.10(1)
Mo8–O4′	2.09(1)	Mo8–O4′	2.08(1)
Mo8–O5′	2.00(1)	Mo8–O15′	1.99(1)
Mo9–O1	2.125(9)	Mo9–O9	2.015(9)
Mo9–O11	2.01(1)	Mo9–O13	1.97(1)
Mo9–O16	2.02(1)	Mo10–O3	2.077(9)
Mo10–O5	2.05(1)	Mo10–O7	2.08(1)
Mo10–O15	2.065(9)	Mo10–O17	2.06(1)
Mo11–O2′	2.03(1)	Mo11–O4′	2.14(1)
Mo11–O5′	2.21(1)	Mo11–O12′	1.92(1)
Mo11–O17	1.91(1)	Ba1–O2	2.75(1)
Ba1–O3	2.844(9)	Ba1–O4	2.842(9)
Ba1–O5	2.76(1)	Ba1–O6	2.729(9)
Ba1–O7	2.92(1)	Ba1–O10	3.032(9)
Ba1–O12	2.96(1)	Ba1–O15	2.92(1)
Ba1–O17	2.65(1)	Ba1–O17′	2.67(1)
Ba2–O3	3.010(9)	Ba2–O6	2.95(1)
Ba2–O7	2.90(1)	Ba2–O8	2.99(1)
Ba2–O9	2.668(9)	Ba2–O10	2.984(9)
Ba2–O11	2.64(1)	Ba2–O13	2.63(1)
Ba2–O14	2.99(1)	Ba2–O16	2.66(1)

[a] Atoms with primed numbers are related to those with unprimed numbers by the inversion center. Cationic bond distances reported using barium, although the cation position is partially occupied by potassium.

TABLE 6
Bond Length–Bond Strength Relationships for $K_{0.19}Ba_{3.81}Mo_{22}O_{34}$

Atom	Σn	Σs	$\Sigma n + \Sigma s$
Mo1	3.43(2)	2.76(7)	6.19
Mo2	3.66(3)	2.39(7)	6.05
Mo3	3.96(3)	2.35(6)	6.31
Mo4	3.30(2)	2.83(7)	6.13
Mo5	3.94(3)	2.42(7)	6.36
Mo6	3.41(3)	2.69(7)	6.10
Mo7	3.84(3)	2.36(7)	6.20
Mo8	3.00(2)	3.01(9)	6.01
Mo9	2.84(2)	3.23(9)	6.07
Mo10	3.26(3)	2.86(8)	6.12
Mo11	2.54(1)	3.30(12)	5.84

Metal–Metal MCE(Σn) = $2\Sigma(\Sigma n)$ = 72.8(5) e^- (w/o intercluster bonds)
Metal–Metal MCE(Σn) = $2\Sigma(\Sigma n)$ = 74.4(5) e^- (with intercluster bonds)
Total valence of Mo_{22} unit = $2\Sigma(\Sigma s)$ = 60(2) v.u.
MCE = (6 × 22) − 60(2) = 72(2) e^-
Formalized oxidation states[a]: (6 × 22) + (34 × 2) + (1 × 0.19) + (2 × 3.81) = 71.8 e^-

[a] Six electrons from each Mo and using the following oxidation states: O^{-2}, K^+, and Ba^{+2}.

these are labeled O4. Oxygens considered O^{i-a} (or O^{a-i}) are edge-bridging between molybdenum atoms of one cluster and terminal to another molybdenum in a neighboring cluster (or vice versa); these include O1, O2, O5, O8, O12, O14, and O15. The general features of the connectivity can be seen in Figs. 2 and 4.

Bond length–bond strength relationships. The Paul ing (24) equation, $d(n) = 2.614 - 0.61 \log (n)$, with $d(1)$(Mo–Mo) = 2.614 Å, has been used to calculate Mo–Mo bond order sums for many ternary reduced molybdenum oxides (12, 21, 25). The numerical values of these calculations for $K_{0.19}Ba_{3.81}Mo_{22}O_{34}$ are found in Table 6. The number of metal-centered electrons (MCE) per $Mo_{22}O_{34}$ cluster can be estimated from the sum of the

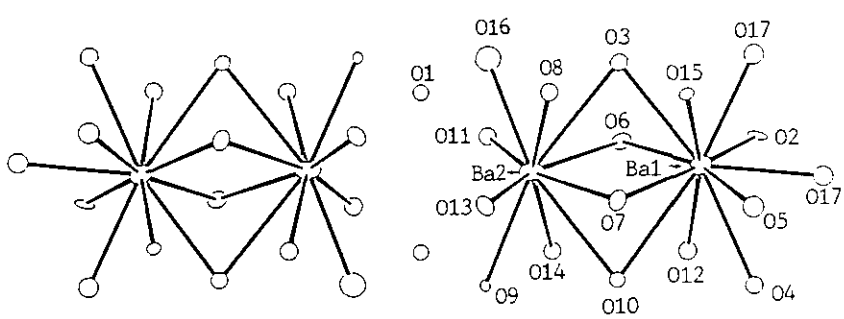

FIG. 3. An ORTEP drawing (70% thermal ellipsoids) of the coordination environments of the barium/potassium cations in $K_{0.19}Ba_{3.81}Mo_{22}O_{34}$.

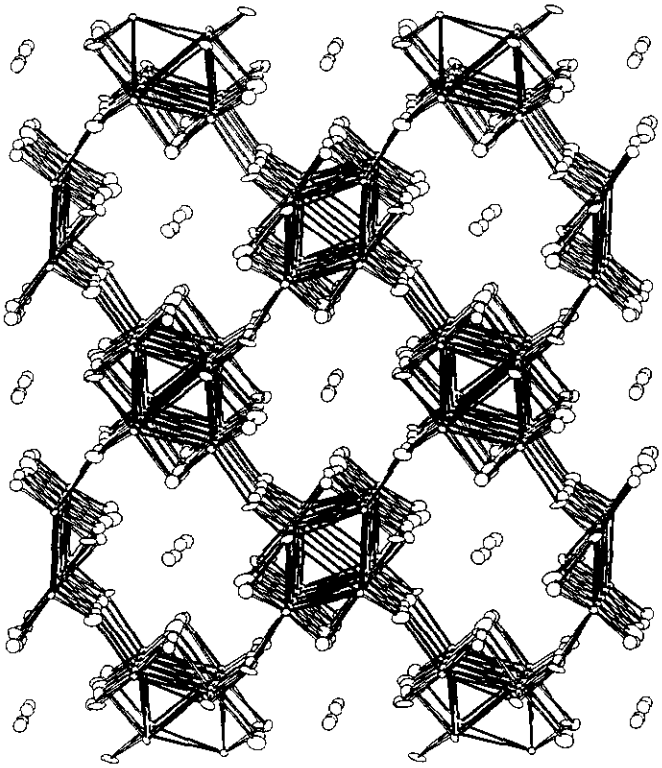

FIG. 4. An ORTEP drawing (70% thermal ellipsoids), as viewed down the c axis, emphasizing the interconnected metal oxide cluster units found in $K_{0.19}Ba_{3.81}Mo_{22}O_{34}$. Cation–oxygen bonds are omitted for clarity.

metal–metal bond orders (n), and results in MCE(2Σ (Σn)) = 74.4(5) if all bonds are included, or 72.8(5) if the intercluster interactions are excluded. These values are higher than expected and probably result from the nonoptimized choice of the Mo–Mo single bond length (21). The sum of the Mo–Mo bond orders and Mo–O bond valences should total six per molybdenum, and the large variance from this value confirms the discrepancy. As can be seen from the values reported in Table 6, this result is most evident for the Mo atoms in the interior positions of the basal plane, which normally show the greatest Mo–Mo bond orders.

The implications of bond length–bond strength calculations for molybdenum oxides has also been well studied (12, 21, 25, 26). The empirical bond valence equation, $s(\text{cation–O}) = [R(\text{cation–O})/R(1)]^{-N}$, developed by Brown and Wu (27) has been used here with values of $R(1)$ and (N), for Mo of 1.882 and (6.0), respectively. The resulting valence for each molybdenum atom is reported in Table 6. A value for the MCE count can be derived from Mo–O bond valence sums by subtracting 2Σ (Σs) (60(2) v.u.) from (6×22) 132, the maximum number of valence electrons available from the molybdenum atoms. The resulting MCE, based on the bond valences, is 72(2).

TABLE 7
The Electron Counts for Selected $M_{n-x}Mo_{4n+2}O_{6n+4}$ and $M_xMo_4O_6$ Phases

Compound	n^a	MCE/Mo[b] (Σs)	MCE/Mo[b] Formal	Reference
$K_{0.19}Ba_{3.81}Mo_{22}O_{34}$	5	3.25	3.26	This work
$In_6Mo_{22}O_{34}$	5	3.30	3.27	(10)
$Ba_3Mo_{18}O_{28}$	4	3.22	3.22	(21)
$Tl_{1.6}Sn_{1.2}Mo_{14}O_{22}$	3	3.24	3.26	(22)
$K_{1.29}Sn_{1.71}Mo_{14}O_{22}$	3	3.14	3.19	(12)
$Sn_{2.3}Mo_{14}O_{22}$	3	3.16	3.18	(12)
$K_{1.66}Pb_{1.34}Mo_{14}O_{22}$	3	3.14	3.17	(12)
$K_3Mo_{14}O_{22}$	3	3.00	3.07	(12)
$Sn_{0.9}Mo_4O_6$	∞	3.35	3.45	(4)
$Pb_{0.77}Mo_4O_6$	∞	3.33	3.39	(3)
$Ba_{0.62}Mo_4O_6$	∞	3.27	3.31	(5)
KMo_4O_6	∞	3.30	3.25	(6–9)
$InMo_4O_6$	∞	3.28	3.25	(2)

[a] Number of Mo octahedra sharing trans edges.
[b] Number of metal-centered electrons per Mo atom, based on bond valence sums[27] and formal oxidation states.

This value is in excellent agreement with the 71.8 e^- expected, based on the formula and formal oxidation states for barium, potassium, and oxygen.

Perhaps the difficulties in synthesizing oligomers with larger values of n can be understood from an electronic viewpoint, based upon MCE. The MCE/Mo for a select group of ternary reduced molybdenum oxides is given in Table 7. The number of electrons available for metal–metal bonding on a per Mo basis is derived from Mo–O bond valence sums and formal oxidation states, respectively. The compounds listed are either oligomers, $M_{n-x}Mo_{4n+2}O_{6n+4}$, or the pure ternary end members with $n = \infty$, $M_xMo_4O_6$. All the $M_xMo_4O_6$ members shown appear to be line compounds, based upon synthetic efforts in this laboratory. Thus for a given cation they represent an optimal electron count for $n = \infty$. A comparison of the oligomeric and infinite chain compounds with similar cations can be made. Increasing the chain length of the oligomers from three to five octahedra raises the electron count to nearly the same levels as found in the corresponding $M_xMo_4O_6$ phases. Thus, members with $n \geq 6$ might be electronically equivalent, and hence, increasingly ustable with respect to the infinite chain compounds.

Utilization of the Brown and Wu equation (27) to determine the valence of the barium and potassium cations, where $R(1)$(Ba–O) = 2.297 and the exponent $N = 7.0$ or $R(1)$(K–O) = 2.276 and $N = 9.1$, gives a value of 2.71(6) for Ba1 and 1.29(4) for K1 if individual bond valences under 0.1 are excluded. The bond valence sums total 2.47(6) for Ba2 and 1.12(4) for K2. Both values are above the expected +2 value for barium, however, similar re-

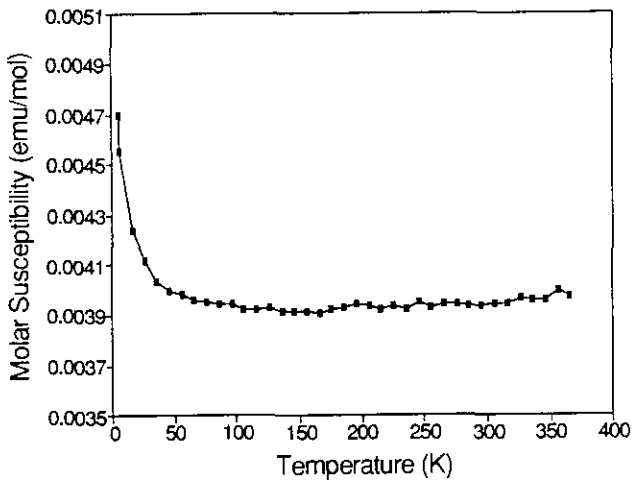

FIG. 5. Molar susceptibility versus temperature of $K_{0.19}Ba_{3.81}Mo_{22}O_{34}$.

sults were obtained for the $n = 1$ cluster, $BaMo_6O_{10}$ (28) (2.6), the $n = 2$ cluster, $Ba_2Mo_{10}O_{16}$ (6) (2.78), and the $n = 4$ cluster, $Ba_3Mo_{18}O_{28}$ (21) (2.56 and 2.34). The high valence derived for the potassium cations is not unexpected since bond valence sums for the two unique potassiums in $K_3Mo_{14}O_{22}$ (13) also gave high values of 1.32 and 1.45. Second, because the concentration of potassium is low in the cation sites of the pentameric member, the cation–oxygen bond distances are primarily valid for barium; therefore, reliable sums cannot be expected for potassium.

Magnetic susceptibility. The magnetic susceptibility of $K_{0.19}Ba_{3.81}Mo_{22}O_{34}$ was measured on selected crystals. These crystals were taken from the same reaction product that yielded the microprobe analytical results. The data were corrected for diamagnetic core contributions, based on the formula determined by the single crystal refinement, using values for the individual ions reported by Selwood (29). The molar susceptibility for this oligomer is displayed in Fig. 5. The susceptibility levels off at ~4000 $\times$ 10^{-6} emu/mol from 56–356 K. This behavior results in a residual susceptibility, due to temperature-independent paramagnetism, χ_{TIP}, of about 180 $\times$ 10^{-6} emu/Mo. This value is higher than the 100 $\times$ 10^{-6} emu/Mo reported for $In_6Mo_{22}O_{34}$ (10). The tail from 6–46 K can be fit by the Curie–Weiss relationship and corresponds to a moment of 0.17 μ_B. The measured moment is too low for the possibility of one unpaired electron for every five formula units (0.77 μ_B) that one might expect from the stoichiometry and formal electron counting. Thus the observed paramagnetic tail most likely arises from an impurity or a defect that results in trapping of an unpaired electron on a cluster. Basically, the cluster units then are all spin-paired as expected. $In_6Mo_{22}O_{34}$, which has essentially the same electron count, was found to have a larger effective moment of 0.9 μ_B. This result is inconsistent with its metallic conductivity and even electron count, and is not presently understood.

Electron spin resonance. ESR data were obtained on the exact material that was used for magnetic susceptibility measurements. The ESR spectrum, taken at 105 K, can be seen in Fig. 6, which shows two peaks which overlap slightly. Their differing peak shapes appear to indicate that they arise from different electronic events. The signal at lower field also has noticeable nuclear hyperfine splitting due to ^{95}Mo and ^{97}Mo ($I = 5/2$). This material was also examined at 7 K, and no significant change in the peak width or signal to noise ratio was observed. However, the hyperfine splitting of the Mo was more clearly resolved. Even at 7 K, neither signal could be power saturated, but some broadening did occur. This result indicates that a very fast relaxation rate dominates the behavior. The ESR results would appear to support

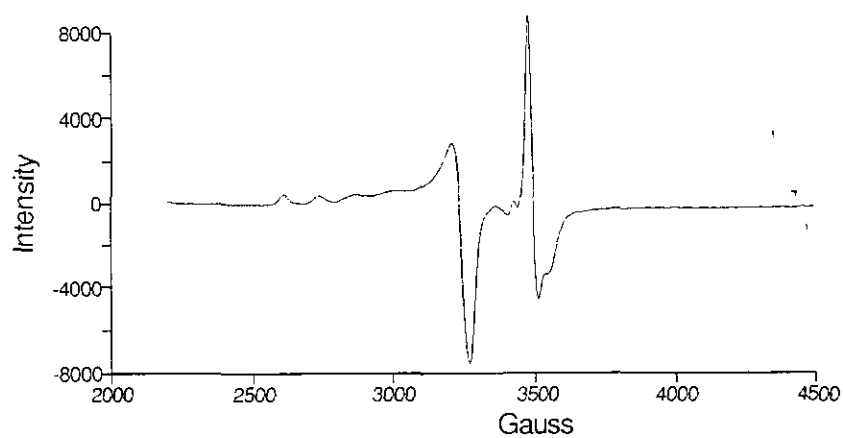

FIG. 6. ESR spectrum at 105 K for $K_{0.19}Ba_{3.81}Mo_{22}O_{34}$.

the presence of molybdenum containing impurities or defects with the odd electron trapped on a single molybdenum atom.

ACKNOWLEDGMENTS

We thank Jim Anderegg for rebuilding the vacuum furnace, without which it would have been difficult to synthesize sufficiently large crystals for this work. Assistance with the magnetic susceptibility and ESR measurements was provided by Jerry Ostenson and Dave Scott, respectively. The microprobe analyses were completed by Dr. Alfred Kracher, Department of Geological and Atmospheric Sciences, at Iowa State University. This work was supported by the U.S. Department of Energy, Office of Basic Energy Sciences, through Ames Laboratory operated by Iowa State University under Contract W-7405-Eng-82.

REFERENCES

1. C. C. Torardi and R. E. McCarley, *J. Am. Chem. Soc.* **101,** 3963 (1979).
2. K. H. Lii, P. A. Edwards, L. F. Brough, and R. E. McCarley, *J. Solid State Chem.* **57,** 17 (1985).
3. C. C. Torardi and R. E. McCarley, *J. Solid State Chem.* **37,** 393 (1981).
4. B. A. Aufdembrink, Ph.D. Dissertation, Iowa State University, Ames, Iowa, 1985. G. L. Schimek, B. A. Aufdembrink, R. E. McCarley, and L. S. Chumbley, manuscript in progress.
5. C. C. Torardi and R. E. McCarley, *J. Less-Common Met.* **116,** 169 (1986).
6. S. C. Chen, Ph.D. Dissertation, Iowa State University, Ames, Iowa, 1991.
7. K. Bauer, F. Rau, W. Abriel, and K.-J. Range, Vortragstagung Fachgruppe Festkörperchemie, Gesellschaft Deutcher Chemiker, Stuttgart, FRG, 1980.
8. K. V. Ramanujachary, M. Greenblatt, E. B. Jones, and W. H. McCarroll, *J. Solid. State Chem.* **102**(1), 69 (1993).
9. R. Hoffman, R. Hoppe, K. Bauer, and K.-J. Range, *J. Less-Common Met.* **161,** 279 (1990).
10. R. Dronskowski, Hj. Mattausch, and A. Simon, *Z. Anorg. Allg. Chem.* **619,** 1397 (1993).
11. Hj. Mattausch, A. Simon, and E.-M. Peters, *Inorg. Chem.* **25,** 3428 (1986).
12. G. L. Schimek, S. C. Chen, and R. E. McCarley, submitted for publication.
13. A. C. T. North, D. C. Phillips, and F. S. Mathews, *Acta Crystallogr., Sect. A* **24,** 351 (1968).
14. G. M. Sheldrick, "Crystallographic Computing 3," Oxford Univ. Press, London/New York, 1985.
15. W. R. Bushing, K. O. Martin, and H. A. Levy, "ORFLS, A FORTRAN Crystallographic Least Squares Program," Report ORNL-TM-305, Oak Ridge National Laboratory, Oak Ridge, Tennessee, 1962.
16. TEXSAN: Single Crystal Structure Analysis Software, Version 5.0, Molecular Structure Corporation, The Woodlands, Texas, 77381, 1989.
17. N. Walker and D. Stuart, *Acta Crystallogr., Sect. A* **39,** 158 (1983).
18. A. Simon, W. Mertin, Hj. Mattausch, and R. Gruehn, *Angew. Chem. Int. Ed. Engl.* **25**(9), 845 (1986).
19. C. K. Johnson, "ORTEP-II, A FORTRAN Thermal-Ellipsoid Plot Program," Report ORNL-5138, Oak Ridge National Laboratory, Oak Ridge, Tennessee, 1976.
20. R. A. Wheeler and R. Hoffmann, *J. Am. Chem. Soc.* **110**(22), 7315 (1988).
21. G. L. Schimek, D. Nagaki, and R. E. McCarley, *Inorg. Chem.* **33,** 1259 (1944).
22. R. Dronskowski and A. Simon, *Acta Chem. Scand.* **45,** 850 (1991).
23. R. D. Shannon, *Acta Crystallogr., Sect. A* **32,** 751 (1976).
24. L. Pauling, "The Nature of the Chemical Bond," 3rd ed., Cornell Univ. Press, Ithaca, New York, 1960.
25. R. E. McCarley, *Polyhedron* **5,** 51 (1986).
26. J. C. J. Bart and V. Ragaini, *Inorg. Chim. Acta* **36,** 261 (1979).
27. I. D. Brown and K. K. Wu, *Acta Crystallogr., Sect. B* **32,** 1957 (1976).
28. K. H. Lii, C. C. Wang, and S. L. Wang, *J. Solid State Chem.* **77,** 407 (1988).
29. P. W. Selwood, *Magnetochemistry,* 2nd ed.; Interscience Publishers: New York, New York, p. 78 (1956).